Journal of Geophysical Research: Space Physics

RESEARCH ARTICLE
10.1029/2018JA025855

Statistical Planetary Period Oscillation Signatures in Saturn's UV Auroral Intensity

A. Bader[1], S. V. Badman[1], J. Kinrade[1], S. W. H. Cowley[2], G. Provan[2], and W. R. Pryor[3]

[1]Department of Physics, Lancaster University, Lancaster, UK, [2]Department of Physics and Astronomy, University of Leicester, Leicester, UK, [3]Science Department, Central Arizona College, Coolidge, AZ, USA

Key Points:
- Saturn's UV auroral intensities are modulated in phase with rotating current systems through all local times and in both hemispheres
- The intensity modulation in each hemisphere is controlled by the superposition of currents originating in both hemispheres
- This marks the first unambiguous evidence of planetary period oscillation-associated field-aligned current flow effects in auroral data

Correspondence to:
A. Bader,
a.bader@lancaster.ac.uk

Citation:
Bader, A., Badman, S. V., Kinrade, J., Cowley, S. W. H., Provan, G., & Pryor, W. R. (2018). Statistical planetary period oscillation signatures in Saturn's UV auroral intensity. *Journal of Geophysical Research: Space Physics*, *123*. https://doi.org/10.1029/2018JA025855

Received 2 JUL 2018
Accepted 26 SEP 2018
Accepted article online 3 OCT 2018

Abstract Saturn's auroral emissions are a good measure of field-aligned current (FAC) systems in the planet's magnetospheric environment. Previous studies based on magnetic field data have identified current systems rotating with the planetary period oscillations (PPOs) in both hemispheres, superimposed onto the local time-invariant current system producing the main auroral emission. In this study we analyze the statistical behavior of Saturn's ultraviolet auroral emissions over the full Cassini mission using all suitable Cassini-UVIS images acquired between 2007 and 2017. We examine auroral intensities by organizing the data by the two PPO coordinate systems. Strong statistical intensifications are observed close to the expected locations of upward FACs in both hemispheres, clearly supporting the main assumptions of the present theoretical model. We furthermore find clear signatures of modulation due to interhemispheric current closure from the PPO system in the opposite hemisphere, although with a weaker modulation amplitude. The auroral intensity in the northern hemisphere is shown to be modulated by a superposition of the FACs associated with both PPO systems, as the modulation phase and amplitude varies as expected for different relative orientations (beat phases) of the two PPO systems.

1. Introduction

Saturn's ring of main auroral emission is located approximately at the open-closed field line boundary (e.g., Cowley et al., 2004). This region maps magnetically to the outer magnetosphere where flow shears between hot plasma populations, subcorotating at different angular speeds with Saturn's planetary rotation, are the largest (e.g., Belenkaya et al., 2014; Hunt et al., 2014). These flow shears are thought to set up a system of field-aligned currents (FACs), of which the upward component is carried by downward electrons precipitating onto the upper atmosphere. The electron impact excitation of hydrogen then generates auroral emissions in a range of wavelengths spanning IR, visible, and UV bands. The same accelerated electron populations are thought to generate the Saturn Kilometric Radio (SKR) emissions through the cyclotron maser instability (e.g., Galopeau et al., 1989).

This largely local time (LT)-fixed FAC system is controlled by internal plasma production and flow as described by the Vasyliunas cycle and by the interaction of Saturn's magnetosphere with the solar wind (e.g., Belenkaya et al., 2011; Cowley et al., 2004, and references therein). How exactly the factors internal and external to Saturn's magnetosphere contribute to the observed LT asymmetries as observed, for example, in ultraviolet and infrared auroral emissions (e.g., Badman, Andrews, et al., 2012; Kinrade et al., 2018; Lamy et al., 2018) remains unsolved. However, it is presumed that the Dungey cycle reconnection near the high-latitude magnetopause occurs mostly in the prenoon sector, leading to larger auroral intensities in this LT regime. This is thought to happen due to a blockage near noon, preventing empty flux tubes returning from the nightside from crossing into the postnoon sector. As the flux tubes can only flow past noon once reconnection has been triggered, auroral emissions could largely be confined to the prenoon sector (Radioti et al., 2017; Southwood & Chané, 2016).

The Kronian aurora is furthermore characterized by many different transient features on both the dayside and nightside of Saturn. These are usually associated with magnetic reconnection events in the magnetotail, the dayside magnetopause, and the cusp (e.g., Badman et al., 2013; Jackman et al., 2013; Meredith et al., 2013). It is also assumed that plasma wave activity, possibly induced by the noon blockage of the plasma return flow, might be responsible for transient brightenings (Yao et al., 2017). Recently, Guo et al. (2018) furthermore observed signatures of near-noon reconnection within Saturn's magnetodisk. These findings indicate that

transient dayside emissions might not only be controlled by solar wind interaction as previously thought but also by the internally controlled Vasyliunas cycle plasma flow.

Furthermore, auroras on Saturn are expected to be modulated by the planetary period oscillations (PPOs). These are periodicities close to Saturn's rotation period which can be observed frequently in all particle, field, and radio wave measurements around Saturn (e.g., Carbary & Mitchell, 2013, and references therein). Possible driving mechanisms for this phenomenon could be a vortical flow structure in the ionosphere of Saturn (e.g., Jia & Kivelson, 2012; Jia et al., 2012) or the plasma pressure of periodically injected energetic particles (Brandt et al., 2010). The PPO behavior can be modeled rather well by two magnetic perturbation fields, one located in each hemisphere and independently rotating in the direction of planetary rotation in both hemispheres at close to the planetary rotation rate—thereby generating a rotating system of FACs superimposed on the LT fixed system thought responsible for the main auroral emission (e.g., Andrews et al., 2010; Provan et al., 2016). These rotating FAC systems were found to produce upward and downward FAC regions mapping to the main auroral oval—modulating the intensity and location of the auroral oval in a sinusoidal manner (Hunt et al., 2014, 2015, 2016).

It has so far been challenging to study the PPO-induced modulation of the Kronian aurora to a significant extent, as this continuous modulation is superimposed on LT asymmetries in the auroral emission pattern, as well as with transient effects like solar wind compressions and sudden reconnection events. First studies investigating a possible intensity modulation of auroral emissions due to the PPO-induced FAC systems' phases have been performed but often produced inconsistent results. A physical association of the UV aurora and SKR emissions has been observed in preequinox HST data (Nichols, Cecconi, et al., 2010). Nichols et al. (2016), using HST imagery from 2011 to 2013, found some modulation of the observed UV intensities in both hemispheres—but as this study was performed on a comparably small dataset with incomplete PPO phase coverage, no hard conclusions could be drawn. An earlier study by Carbary (2013) used Cassini UVIS imagery from 2006 to 2009 to investigate rotational modulation of Saturn's auroral intensities with respect to SKR phase, but observed clear dependencies only for the southern hemisphere. Lastly, Badman, Andrews, et al. (2012) observed rotational modulation of infrared emissions in Cassini VIMS data between 2006 and 2009, although out of phase with the expected auroral response.

In this study, we expand on the previous investigations of auroral modulation due to PPO influences. Section 2 presents a short background on the ongoing investigations of PPO and the reference frames used in this study. Drawing on the full Cassini UVIS data set covering the time span from 2007 to 2017, described in section 3, we are able to statistically investigate auroral intensity modulations in great detail. The results of this analysis are presented in section 4. Finally, we summarize and discuss our findings and their implications for present theoretical models in section 5.

2. The PPO Systems and Their Reference Frames

With the arrival of Cassini at Saturn, it became clear that most magnetospheric data exhibit oscillatory signatures at rates close to Saturn's rotation rate. After Kurth et al. (2008) had found two distinct SKR rotation periods, Gurnett et al. (2009) suggested that these emanate from the two polar hemispheres of Saturn. Extensive studies showed that in the northern (southern) polar cap regions, only magnetic field oscillations due to the northern (southern) PPO system are observed (Andrews et al., 2012), but in the equatorial regions, a superposition of both systems' oscillations is found (Provan et al., 2011). Provan et al. (2018) observed southern oscillations in the northern hemisphere on the proximal and F-ring orbits. Such interhemispheric coupling is believed to be observed on these orbits due to the trajectory of Cassini, where the spacecraft moves very close to the FAC regions. The relative amplitude of the two systems has been found to vary over time (Provan et al., 2013), which can largely be attributed to seasonal effects (Provan et al., 2015) and, to some degree, changes in the upstream solar wind properties (Zarka et al., 2007). From mid-2013 to mid-2014, the two PPO systems have been shown to rotate in coalescence, locked nearly in relative antiphase (Provan et al., 2016).

Both PPO systems are thought to be associated with a system of rotating current systems, with currents flowing into one side of the ionosphere along the magnetic field, crossing the polar cap as ionospheric Pedersen currents and returning outward into the magnetosphere as FACs on the other side. Current closure is expected to occur partly in the equatorial plane in the outer magnetosphere and partly in the opposite hemisphere. In each hemisphere's ionosphere, currents associated with either PPO system flow on the same field lines and are therefore not latitudinally separated (e.g., Bradley et al., 2018; Hunt et al., 2015). A comprehensive and illus-

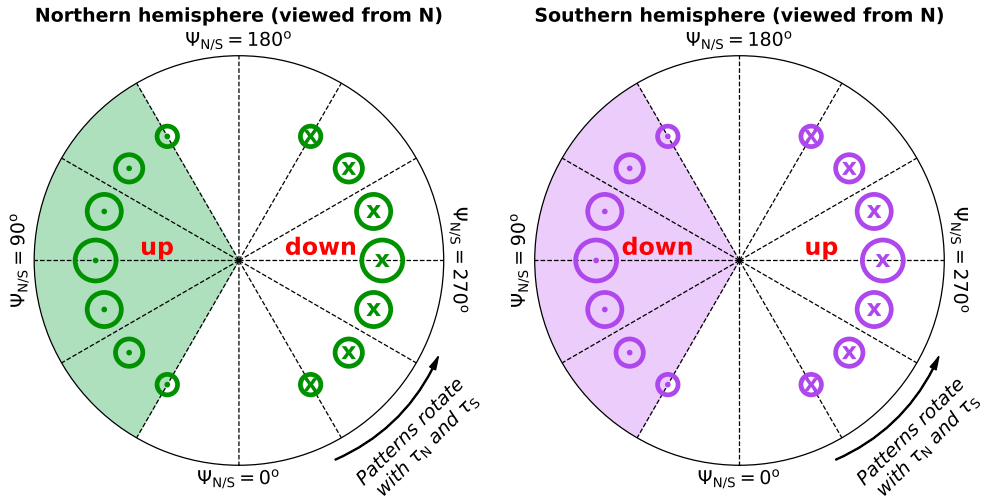

Figure 1. Sketch of the PPO-related rotating FAC patterns in Saturn's polar ionosphere. To the left (right), the northern (southern) polar region is shown as viewed from above the north pole. With the near-equatorial PPO perturbation fields directed toward the bottom of the figure, $\Psi_{N/S}$ increases in clockwise direction. Green/purple-circled crosses and dots represent FACs flowing into and out of the plane of the diagram, respectively. For example, in the northern hemisphere, upward FACs and therefore increased auroral intensities are expected at around $\Psi_N = 90°$ and at around $\Psi_S = 90°$. The relative orientation of the two PPO systems determines whether their associated upward FAC regions are colocated or not. PPO = planetary period oscillation; FAC = field-aligned current.

trated description of these current systems is given in, for example, Hunt et al. (2015). Both these PPO systems can be modeled with horizontally orientated dipole fields and rotate azimuthally in the direction of planetary rotation with their respective PPO rotation rates $\tau_{N/S}$. The orientation of each system is hereby defined by the counterclockwise azimuthal angle of the equatorial perturbation field $\Phi_{N/S}(t)$. This angle is referenced to local noon, increases in the direction of planetary rotation, and is often referred to as PPO dipole angle or phase angle.

For locating an auroral feature in this rotating frame, a PPO "longitude" system can then be defined with $\Psi_{N/S}(\varphi, t) = \Phi_{N/S}(t) - \varphi$ with φ as the LT-referenced planetary longitude. The location of a feature is therefore referenced to the PPO system's dipole orientation $\Phi_{N/S}(t)$ at a specific time t. An auroral feature rotating with the same speed as the PPO dipole, for example, would therefore have a constant $\Psi_{N/S}$ value.

From the PPO model initially proposed by Andrews et al. (2010) and more recently described by Hunt et al. (2015), it is clear that the associated FACs will have different strengths and flow directions at different $\Psi_{N/S}$. The expected FAC patterns are sketched in Figure 1. In the northern hemisphere, the upward FACs are expected to maximize close to $\Psi_N = 90°$ for the northern (primary) PPO system, with the downward currents maximizing around $\Psi_N = 270°$. Interhemispheric currents from the southern (secondary) PPO system closing the northern hemisphere are thought to cause the same FAC pattern, with upward currents maximizing near $\Psi_S = 90°$ and downward FACs peaking around $\Psi_S = 270°$. Conversely, upward FACs are expected to maximize close to $\Psi_{S/N} = 270°$ and downward FACs near $\Psi_{S/N} = 90°$ in the southern hemisphere (Hunt et al., 2015). With auroral brightness being directly related to upward currents associated with downward-precipitating electrons, we therefore expect to observe relatively higher auroral intensities at $\Psi_{N/S} = 90°$ for the northern hemisphere and $\Psi_{N/S} = 270°$ for the southern hemisphere and relatively lower intensities on the other side of the polar cap.

The relative strength of the current systems associated with the primary and secondary PPO systems changes with season (Provan et al., 2013). Over the course of the Cassini mission, the two PPO systems switched dominance several times, with often one system being stronger than the other by a factor 2 or larger. In case of equal strengths, we expect the primary PPO system to dominate the rotational modulation of the UV auroral intensity in each hemisphere, since the secondary system's currents are partly closed in the equatorial plane. Bradley et al. (2018) found that about half the current associated with each PPO system is closed in the equatorial plane, while the remaining half closes in the opposite hemisphere—the FACs in each hemisphere are therefore expected to be modulated twice as strongly by the primary than by the secondary PPO system. If however the strengths of the two PPO systems differ significantly, the currents associated with the dominat-

ing system and crossing over into the other hemisphere might be as strong or even stronger than the currents associated with the (primary) PPO system in that hemisphere. For a more detailed description, the reader is referred to, for example, Nichols et al. (2016).

3. Data Set

3.1. General

This study is based on the complete data set of auroral imagery obtained by the Cassini UVIS spectrographic imager (Esposito et al., 2004) between orbit insertion on 1 July 2004 and end of mission on 15 September 2017. The UVIS instrument consists of two telescope-spectrographs covering the wavelength ranges 56–118 nm (extreme ultraviolet) and 110–190 nm (far ultraviolet or FUV). All observations used in this study have been taken with the FUV channel.

The UVIS FUV sensor consists of 64 × 1,024 pixels, providing 64 spatially distinct spectra arranged along a single line. Each of the 64 spatial pixels has an angular resolution of 1.0 × 1.5 mrad. A two-dimensional pseudo-image is obtained by slowly slewing the spacecraft such that the detector sweeps over the area of interest. Depending on the apparent size of the auroral oval from the spacecraft's point of view, repeated sweeps may be necessary to attain full coverage of the auroral region. Latitude-longitude grids of each image are calculated by projecting each pixel onto an ellipsoid located at an altitude of 1,100 km above Saturn's 1 bar level ($R_E = 60,268$ km, $R_P = 54,364$ km)—the altitude at which auroral emissions are thought to be generated (Gérard et al., 2009). This is performed using Cassini SPICE pointing information available on the Planetary Data System.

During one exposure, each spatial pixel provides an intensity spectrum with a resolution of up to 1,024 spectral bins equally spread over the 110–190-nm range. In order to obtain the total unabsorbed H_2 emission in the 70–170-nm range, we first determine the brightness in the 155–162-nm range from the measured spectra. Multiplying the resulting intensity by the factor 8.1 then gives the unabsorbed H_2 emission intensity over the whole UV wavelength range (Gustin et al., 2016, 2017).

After discarding images with poor coverage of the auroral region and unsuitable viewing geometries, we are left with 4,192 images suitable for our analysis. From mid-2013 to mid-2014, the northern and southern PPO systems were rotating at the same rate, locked in near antiphase (Provan et al., 2016). Images taken during this interval would therefore introduce a strong statistical bias, as the two phase systems are not quasi-independent anymore. We therefore exclude all imagery taken during this time from our data set, leaving us with 2,777 images—still a much larger set than used in comparable previous studies.

The PPO phase for each UVIS image was determined using the most recent PPO model described in Provan et al. (2018). The initial determination of the PPO phase values employed in this study includes some inherent uncertainty due to the use of sliding windows with a size of several months, but the errors are relatively small and well described in the corresponding publications (e.g., Provan et al., 2016, 2018).

Additional inaccuracies are introduced due to the exposure time of UVIS UV imagery. High-resolution scans can take up to 3 hr—during this period, the PPO phase $\Phi_{N/S}(t)$ will have changed by more than 90°. Different pixels covering the auroral oval have likely been measured at different PPO phase angles, and the PPO phase used in our calculations might in some extreme cases be in error by up to 45° (the center time of the UVIS exposure is used to define its corresponding PPO orientations). These are rather rare cases, however—the mean exposure time of all imagery used is below 1,000 s, resulting in a PPO phase angle change of less than 10° throughout the exposure of a typical image. With a large enough data set like ours, we therefore expect these effects to largely average out.

3.2. Temporal and PPO-Phase Sampling

As most UVIS imagery has not been collected continuously but only in campaign-style whenever Cassini's orbital position was favorable and there was a justifiable scientific interest, the temporal coverage of the data set is very uneven. Figure 2 shows the number of images per year used in this study for both hemispheres. The number of images varies strongly throughout the mission, with, for example, only ~20 images from 2009 but close to 1,000 from the second half of 2014 for the northern hemisphere (imagery between 2014-0 and 2014-180 having been excluded due to the PPO phase lock as indicated in section 3.1). During the years 2010–2012, no UVIS images are available as Cassini's orbit was positioned mostly in the equatorial plane, and Saturn's polar regions were simply not visible to the instrument. Overall, we therefore cannot take into account

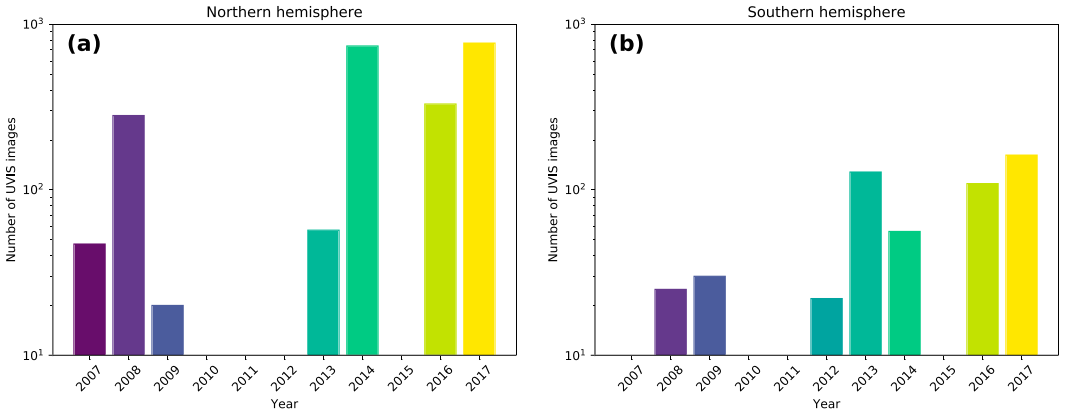

Figure 2. Number of UVIS images available for this study, (a) for the northern and (b) for the southern hemisphere. Note the logarithmic scale of the *y* axis. The temporal sampling is clearly quite uneven, with the years 2009–2012 providing barely any auroral imagery useful for our purpose.

temporal changes in relative PPO strengths and rotation rates between the two perturbation fields in any significant manner, apart from excluding the statistically biased data from mid-2013 to mid-2014 coalescence period as noted above. Note the unequal coverage between the northern and southern hemispheres—our data set encompasses 2,245 images in the north and 532 in the south.

Figure 3 shows the distribution of the used images across different PPO phase angles $\Phi_N(t)$ and $\Phi_S(t)$. As uneven as the temporal coverage may be, the full range of PPO phase angles has been sampled quite evenly

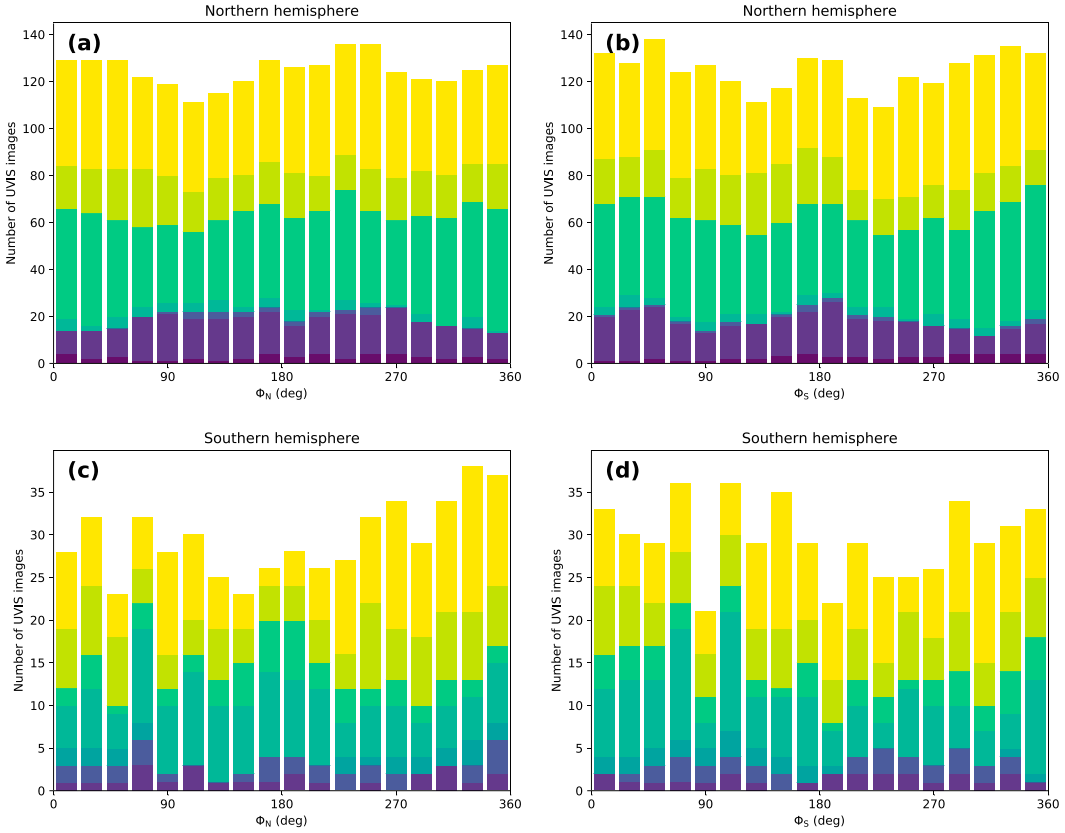

Figure 3. Coverage of planetary period oscillation phase angles $\Phi_{N/S}$ in both hemispheres; same data set as shown in Figure 2. (a) and (b) show the number of UVIS images per planetary period oscillation phase angle Φ_N and Φ_S bin, respectively. (c) and (d) show the same statistics for the southern hemisphere. The color scale in all plots corresponds to the year-coloring in Figure 2. Note the different vertical scaling between the top and bottom plots.

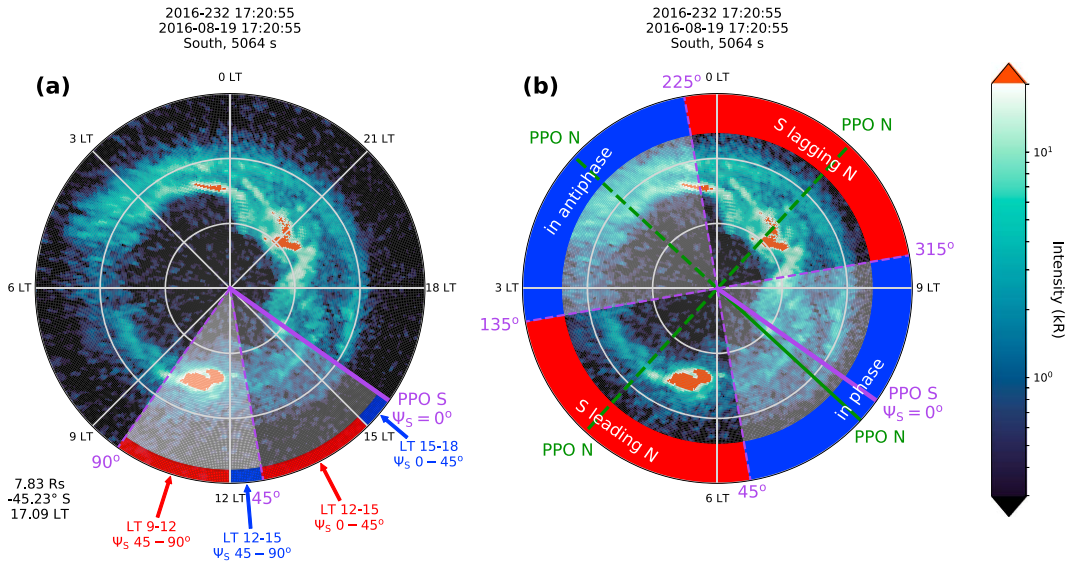

Figure 4. Example UVIS image of the southern hemisphere from 2016-232 on which the binning procedures are visualized. The view is from the above the north pole, looking "through" the planet into the southern hemisphere; the Sun/noon is toward the bottom of the figure. Concentric rings around the pole mark 10° colatitude steps. Information about Cassini's location (radius, latitude, and LT) is given in the bottom left corner; time stamp, hemisphere, and exposure time are given on top. Note the logarithmic intensity scale. (a) shows a 3-hr LT grid superimposed on the original image, with two exemplary PPO bins (45° bin size) overlaid in shades of white (the actual bin size used for this study is 4/3 h, and 20°, respectively. The orientation of the southern PPO system for this time period is indicated by a bold purple line, by definition coinciding with $\Psi = 0°$. The superposition of the LT and PPO bin grids creates a pattern of LT-PPO bins of alternating sizes; marked in blue and red and annotated accordingly. (b) defines the beat phases of the two PPO systems. Red and blue sections mark which beat phase this image would correspond to depending on the orientation of the northern PPO system. The actual orientation of the northern PPO system for this time stamp is marked in green, this image would therefore be assigned the beat phase *in phase*. Note that the beat phase does not depend on which hemisphere one considers, it is well defined only by comparing the orientations of the two PPO systems. PPO = planetary period oscillation; LT = local time.

in the northern hemisphere due to the large number of images. The coverage in the south is more uneven, but all PPO phases have been sampled a number of times.

4. Analysis

When analyzing the modulation of the auroral intensity due to the two rotating PPO systems, one has to take into account the clear LT differences which the Kronian aurora statistically exhibits (e.g., Grodent et al., 2005). In order to separate LT and PPO modulation as well as possible, we analyze the auroral intensity in an LT-PPO phase space—similar to previous studies using HST and Cassini VIMS data (Badman, Achilleos, et al., 2012; Nichols et al., 2016). The binning algorithm employed in this study is illustrated in Figure 4a. Each image is sectioned in longitude according to a combination of equally sized LT and PPO $\Psi_{N/S}$ binning grids. We choose bin sizes of $\Delta LT = 4/3$ hr and $\Delta\Psi_{N/S} = 20°$, respectively, resulting in 18 LT and 18 PPO "magnetic longitude", $\Psi_{N/S}$, bins. Note that superposing these two grids leads to the image being sectioned in 36 sections of alternating size as shown in Figure 4a. Each section is averaged in longitude before its intensity maximum is determined; all these maxima of all relevant images are then sorted into LT-PPO bins. The average intensity maximum in each LT-PPO bin is then calculated by taking a mean of all values in the corresponding bin.

The LT-PPO intensity histograms for the northern hemisphere are shown in Figure 5. Both histograms are based on the same set of 2,245 UVIS images of the northern aurora. A first look at the LT histogram on the top of both plots shows the typical LT distribution of the Kronian auroral intensity, with a clear peak near dawn and a small bump between dusk and midnight. This agrees with previous studies of both the UV (e.g., Kinrade et al., 2018; Nichols et al., 2016) and IR auroral emissions (Badman, Andrews, et al., 2012). The secondary emission peak behind dusk could be associated with periodic auroral spots caused by magnetopause reconnection or Kelvin-Helmholtz waves (e.g., Mitchell et al., 2016).

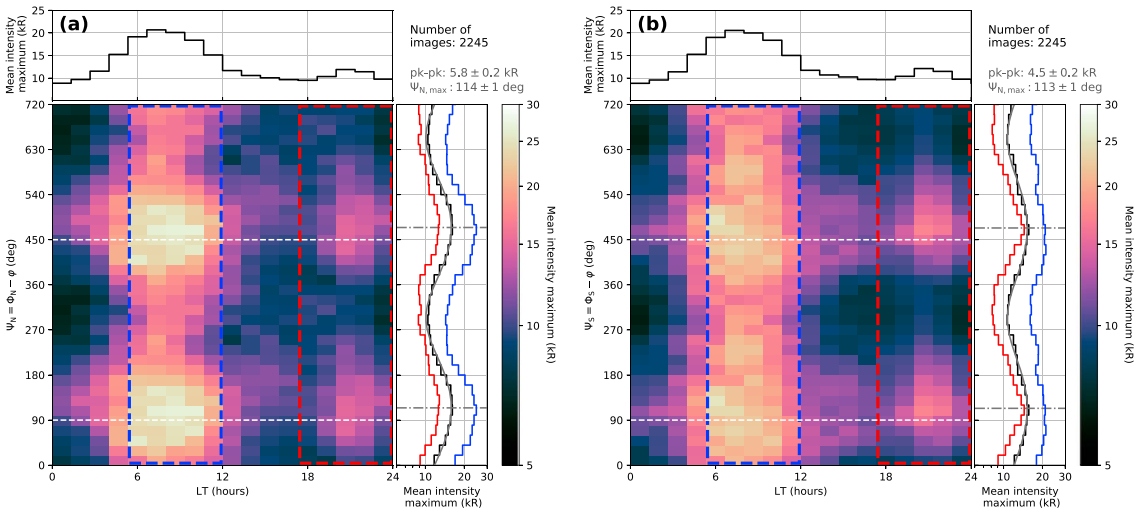

Figure 5. Mean of northern UV auroral intensity maxima per local time (4/3-hr bin size) and PPO phase $\Psi_{N/S} = \Phi_{N/S} - \varphi$ (20° bin size), shown in a logarithmic color scale. (a) Northern hemisphere auroral intensity ordered by the northern PPO system and (b) northern hemisphere auroral intensity ordered by the southern PPO system. Two Ψ phase cycles are plotted for clarity; the expected locations of maximum upward current are indicated by white-dashed lines. On the top and to the side of each 2-D histogram, the averages of the mean intensity maxima over the $\Psi_{N/S}$ and LT dimensions are shown in black, respectively. Separate histograms showing the PPO intensity modulation in the dawn-noon (blue) and dusk-midnight (red) regions are calculated from the accordingly marked parts of the histogram and shown to the right side (note the logarithmic intensity scale). The histogram over the full LT range (black) has been fitted with a simple sine (gray). Its maxima are marked with vertical dash-dotted lines; its peak-to-peak (pk-pk) amplitude and the Ψ_N angle with the highest intensity are given in the top right corner of each figure.

More interestingly, the northern auroral intensity shows a clear modulation in terms of both Ψ_N and Ψ_S. In Figure 5a, showing the auroral intensity ordered by LT and Ψ_N, the mean auroral intensity maximum varies with a peak-to-peak amplitude of about 5.8 kR. We find the sinusoidal fit on the histogram to maximize at $\Psi_N = 114°$, slightly lagging behind the expected location where maximum upward FAC is expected to occur, at $\Psi_N \approx 90°$ (e.g., Andrews et al., 2010; Hunt et al., 2014). This intensity modulation is however significantly higher and more ordered than observed in previous studies (Badman, Achilleos, et al., 2012; Nichols et al., 2016). The modulations are most intense near dawn (blue box/histogram) but clearly also present between dusk and midnight (red box/histogram). The phase of the modulation is largely consistent through LT and fits reasonably well to the regions of FACs identified by Hunt et al. (2014) using Cassini MAG data.

The northern auroral response associated with interhemispheric current closure of the southern PPO system, shown in Figure 5b, is very similar to the modulation imposed by the primary system. The peak-to-peak intensity modulation amplitude is approximately 4.5 kR, slightly smaller than what we observe for the primary system, and the peaks themselves seem less pronounced in Ψ_S. The intensity maxima are again located close to their expected location at $\Psi_S \approx 90°$ throughout all LTs, with the highest intensities occurring at $\Psi_S = 113°$.

In the southern hemisphere, considerably fewer UVIS images were available for this analysis—only 532 images, about 24% of what were used from the northern hemisphere. The corresponding histograms are shown in Figure 6. Nevertheless, modulations both due to the primary (Figure 6b) and secondary (Figure 6a) PPO system are clearly visible and mostly consistent with what was observed in the north. Again, intensity maxima in the primary (secondary) PPO system are found at $\Psi_S = 299°$ ($\Psi_N = 317°$) close to their expected locations at $\Psi_{N/S} \approx 270°$, and the amplitude of the modulation is slightly higher for the primary PPO system (5.6 kR) than for the secondary one (4.2 kR). It does seem that the modulation phase is slightly shifted between the dawn-noon and dusk-midnight sectors, although this might well be an effect due to the much smaller size of the data set compared to the northern hemisphere.

A feature shared between all the histograms shown however is the shift of the intensity peak in $\Psi_{N/S}$ relative to where the largest FACs are expected from the initial model deduced by Andrews et al. (2010), sketched in Figure 1. In both hemispheres and for both the primary and secondary PPO modulation, the intensity peak is consistently observed at larger $\Psi_{N/S}$ than expected from this model. The offset is in the range of $\Psi_{max} - \Psi_{N/S} \approx 25–50°$ in most histograms, such that the intensity maximum is always lagging behind the expected FAC maximum. Supporting this offset, Hunt et al. (2014) observed the magnetic signatures of the parallel upward

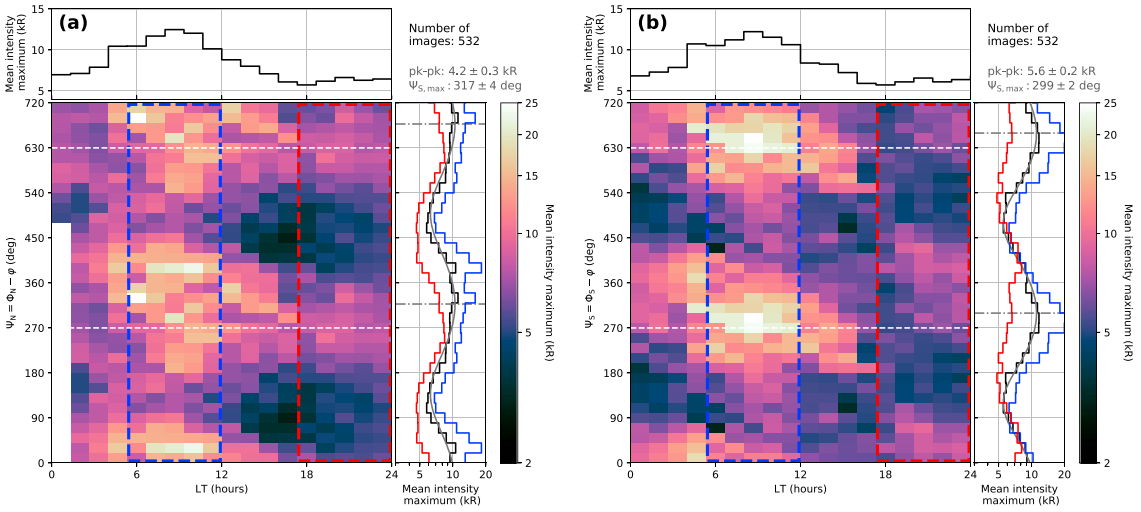

Figure 6. Mean of southern UV auroral intensity maxima per local time and PPO phase $\Psi_{N/S} = \Phi_{N/S} - \varphi$, in the same format as Figure 5. (a) Southern hemisphere auroral intensity ordered by the northern PPO system and (b) southern hemisphere auroral intensity ordered by the southern PPO system. Note the different intensity scales compared to Figure 5. PPO = planetary period oscillation.

current density of the main current sheet in the southern hemisphere to maximize at roughly $\Psi_S \approx 300°$, perfectly fitting to the intensity maximum in Figure 6b. In the northern hemisphere, the exact phase Ψ_N at which the upward current density maximizes was not determined (Hunt et al., 2015)—assuming a similar lag as in the southern hemisphere, the upward current can be expected to maximize at $\Psi_S \approx 120°$, coinciding very closely with the location of the observed UV intensity maximum we find (Figure 5a). It is unclear how this lag between the expected (Andrews et al., 2010) and observed FAC maxima, seen in both the magnetic field data (Hunt et al., 2014) and auroral emissions, can be explained.

We also want to note here that the auroral intensifications we observe in Figures 5 and 6 are not necessarily caused directly by PPO-associated FAC maxima rotating around the planet. PPO modulations pervade the entire magnetosphere and therefore entail a whole host of magnetospheric dynamics which could influence the auroral intensity in a periodic manner. The most obvious or best explored process in this context might be magnetotail reconnection, the occurrence of which is ordered by PPO phase (Jackman et al., 2016). Magnetotail reconnection events have been shown to occur preferentially at $\Psi_N \approx 0/360°$ and at $\Psi_S \approx 90°$, that is, they happen preferentially ~90° ahead in phase of the peak in the upward current for both PPO systems. With magnetotail reconnection generally causing short-lived and localized intense auroral features (Jackman et al., 2013), we would also observe statistical brightenings of the UV aurora at certain PPO phases—depending on the reconnection site as well as the lifetime and corotation speed of the associated auroral feature.

We have no means of separating direct PPO FAC-related auroral intensifications from indirect ones caused by PPO-modulated magnetospheric dynamics, and the impact of indirectly caused intensifications on our results cannot be judged reliably. The size of the data set and the typically rather low exposure time of the UVIS images compared to the occurrence rate of tail reconnection may seem to indicate that the fraction of images in which associated auroral emissions are observed is rather small—but depending on their lifetime, these auroral features might (sub)corotate for a significant time and, for example, lead to an auroral intensification when passing through dawn, "compromising" whole imaging sequences with indirect auroral brightenings.

The large number of UV images in the north additionally provides us with the chance to further investigate interactions between the primary and secondary PPO systems. In order to look at the interhemispheric interactions in more detail, we split the data set in four groups according to the relative orientation of the two PPO systems, the *beat phase*. Each image is binned into *in phase*, *in antiphase*, *S leading N*, and *S lagging N* beat phase bins as demonstrated in Figure 4b.

Depending on the beat phase, one can expect some overlaps between the FACs of both PPO systems, enhancing or attenuating the overall FACs flowing at certain $\Psi_{N/S}$. A sketch illustrating the anticipated behavior in the northern hemisphere is shown in Figure 7. Note that the latitudinal offsets of the current regions shown are

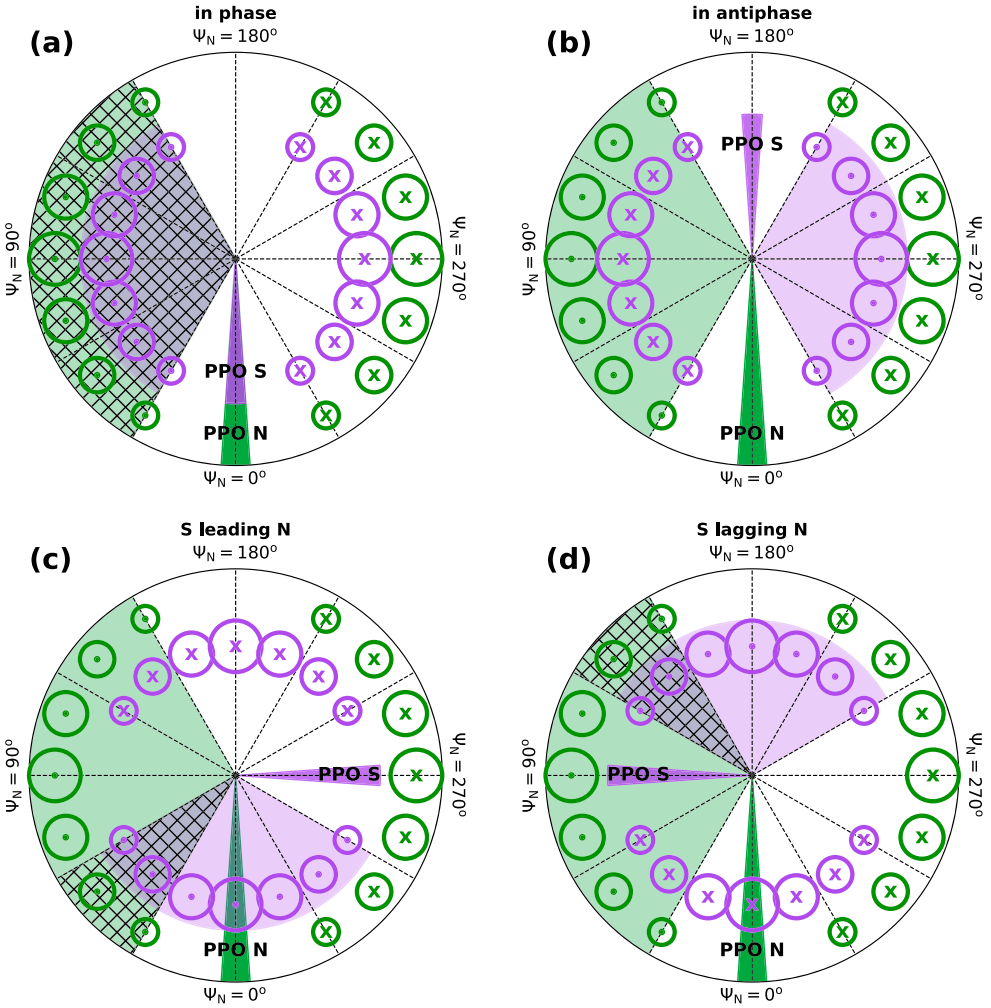

Figure 7. Sketch of expected FAC flows in the northern hemisphere for different beat phases. The view is onto the north pole, with the observer rotating with the primary PPO system (PPO north, in green). The northern PPO perturbation field is directed toward the bottom of each plot, with "magnetic longitude" Ψ_N increasing in clockwise direction. The relative orientation of the secondary PPO system (PPO south) is marked in purple. Circles with dots represent upward FACs, while circles with crosses indicate downward FACs; both colored according to the PPO system they are associated with. The radial/latitudinal offset of the FAC markers for both systems is only for clarity; in reality, both systems' FAC regions map to similar latitudes (e.g., Hunt et al., 2015). Regions where both systems' upward FACs overlap are highlighted with hatching. (a) shows how the upward FACs of the two PPO systems overlap around $\Psi_N = 90°$ if they are beating *in phase*, increasing the overall current density and leading to an enhancement of the intensity modulation expected due to the primary PPO system. At the same time, downward currents on the other side of the pole overlap. (b) In antiphase, the primary PPO upward FAC region coincides with the secondary PPO downward FAC region and vice versa; attenuating the modulation of auroral intensity due to the primary PPO system. (c) and (d) show overlaps between the two rotating FAC systems for the intermediate beat phases *S leading N* and *S lagging N*. The overlaps are thought to create regions of enhanced upward FACs offset to smaller/larger Ψ_N angles than expected if only primary PPO modulation was present. PPO = planetary period oscillation; FAC = field-aligned current.

only for clarity and have no physical background (the reader shall be reminded that FACs associated with both the primary and secondary PPO system flow on the same field lines, i.e., map to the same latitude; ; Bradley et al., 2018; Hunt et al., 2015). If both PPO systems are aligned *in phase* (Figure 7a), an increase in the FAC modulation due to the primary PPO system can be expected, while in the case of antiparallel orientation (*in antiphase* Figure 7b), the modulation should be attenuated by a factor depending on the relative strength of the two current systems at that time. For the intermediate beat phases (Figures 7c and 7d), shifts of the peak upward FAC regions caused by primary PPO modulation to lower (higher) Ψ_N are expected for PPO S leading (lagging) PPO N.

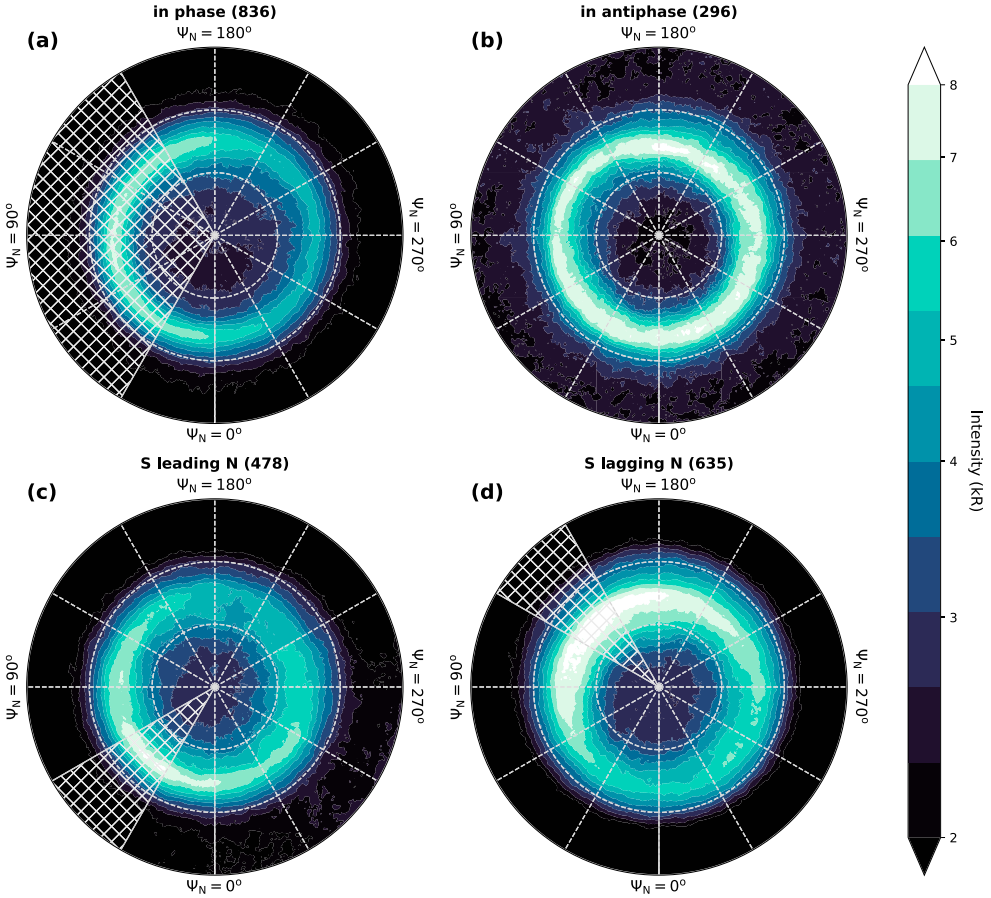

Figure 8. Contour plots of the median northern auroral intensity in the PPO north frame, for the four different beat phases. The format is the same as in Figure 7, with (a) the mean of all images taken while the two PPO systems were in phase and (b) for the *in antiphase* case. (c) and (d) show the mean auroral intensity for the *S leading N* and *S lagging N* beat phases, respectively. The white-hatched regions are very rough estimates of where the upward current regions of the northern (primary) and southern (secondary) PPO systems overlap and the UV auroral emission is expected to increase, as explained in Figure 7 and the accompanying text. Numbers in parentheses correspond to the number of UVIS images on which each median image is based. PPO = planetary period oscillation.

Figure 8 shows the average auroral emissions observed in the northern hemisphere. Each plot shows the mean of all UVIS images of the northern auroral oval and used in this study which were obtained when the two PPO systems were orientated *in phase*, *in antiphase*, and so on. If both PPO systems are aligned *in phase* (see Figure 8a), we find a clear increase of the auroral emission strength close to $\Psi_N = 90°$; directly opposite, we observe a strong depression in the emission strength near $\Psi_N = 270°$. This whole pattern is, as already observed previously, tilted to slightly larger Ψ_N than expected.

Figure 8b shows that the auroral emissions are considerably less ordered in the northern PPO frame if the northern and southern PPO systems are orientated in relative *antiphase*. While we expect the intensity maximum to be lower than for the *in phase* case, this cannot be observed. Instead, the emission is mostly unordered in Ψ_N, and the mean overall intensity seems to be higher compared to when the two PPO systems are *in phase*. It is to note however that the set of images on which Figure 8b is based is less than half the size of the set corresponding to Figure 8a. And while the number of images may still seem quite large, it is worth mentioning again that these are by no means continuous data sets. Of the 296 UVIS images used in Figure 8b, 73 have been acquired on 2014 DOY 289-290 and 56 on 2008 DOY 201. This strong grouping of images is on one hand fortunate, as it allows us to track several planetary rotations and directly investigate PPO-related modulations under near constant magnetospheric conditions. On the other hand, this obviously introduces a clear bias toward effects external to PPO such as different solar wind input between different image groups, and the absolute intensities between the different beat phase averages are therefore not really comparable.

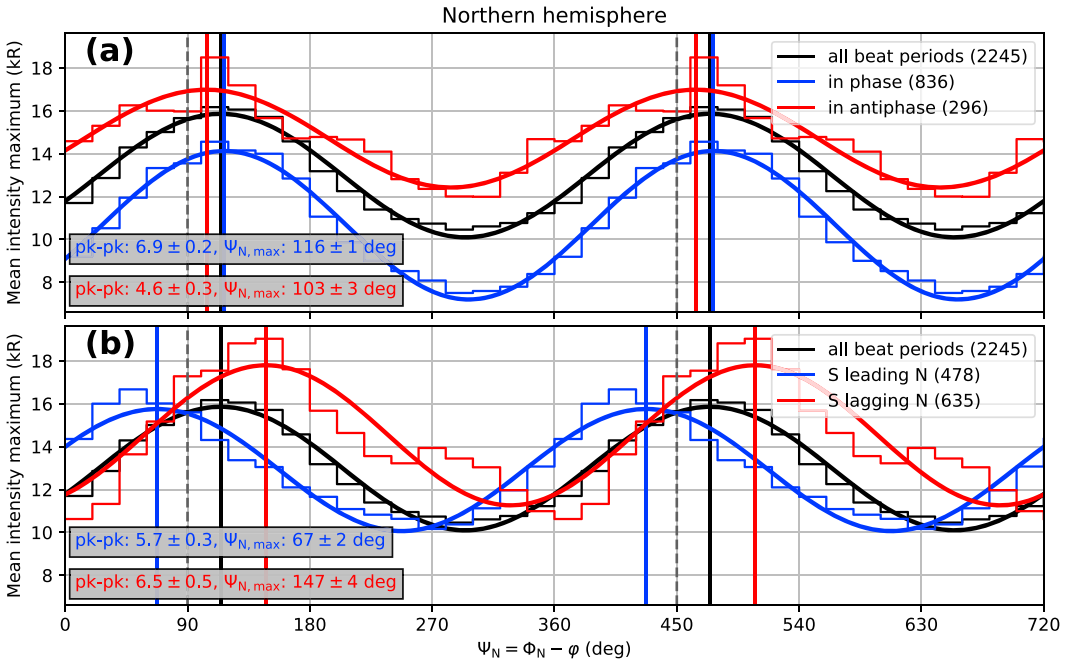

Figure 9. Comparison of Ψ_N versus mean intensity maximum histograms for different PPO beat phases for auroral observations in the northern hemisphere, ordered by the northern PPO system. Again, two Ψ_N cycles are shown for clarity. (a) compares the overall intensity modulation (black) with the modulations observable when the northern and southern PPO systems are in phase (blue) and when they are in antiphase (red). Numbers in parentheses show the number of UVIS images included in each subset. Note that the black line plot is identical to the black plot in the right side histogram in Figure 5a. The three histograms have been fitted with a simple sinusoid to clarify similarities and differences in modulation phase and amplitude. The fits' peak-to-peak modulation amplitudes and phases are given in boxes in the bottom left corner. The locations where maximum upward FACs are expected are marked with vertical-dashed lines. (b) is of the same format, comparing the northern auroral intensity modulations when the southern PPO system is leading (blue) or lagging (red) the northern PPO system with respect to the direction of planetary rotation. PPO = planetary period oscillation; pk-pk = peak-to-peak.

In Figures 8c and 8d, we see the observed auroral maximum in the northern PPO frame to be clearly displaced from its average location at about $\Psi_N = 90°$. As the hatched regions indicate, the displacement follows the direction predicted by the simple model of overlapping currents described in Figure 7. Please be aware that the hatched regions are only an approximation to guide the eye, and their width and location are by no means exact or based on any observations or calculations.

We now perform the same intensity analysis as shown previously (e.g., Figure 5) but this time, for a separate data set for each beat phase. Here we focus on analyzing the auroral intensity modulation in the northern hemisphere due to the northern PPO system (i.e., we calculate histograms identical to the one shown in Figure 5a with beat phase subsets of the full data set). For brevity, the full histograms are not shown—we only compare the LT-averaged histograms such as found, for example, on the side of Figure 5a. A comparison of these histograms for the different beat phases is shown in Figure 9. Figure 9a compares the averaged auroral intensity maximum of the *in phase* and *in antiphase* beat phases to the overall intensity histogram shown in Figure 5a. For clarity, all histograms have been fitted with a simple sinusoid. It is clear that the phase of the primary PPO-induced modulation does not shift noticeably, but the amplitude of the modulation is enhanced if both PPO systems beat *in phase* compared to when they are in relative *antiphase*. The modulation amplitude for the latter case is comparable to the overall modulation amplitude drawn in black. The intensity baselines of the colored curves are significantly offset, with the *in phase* intensities oscillating about an average intensity maximum of approximately 10 kR and the *in antiphase* curve being centered on approximately 15 kR. This difference might well be explained by the comparably small number of *in antiphase* images, making the overall histogram visibly noisy and possibly introducing a bias toward certain time periods, solar wind conditions or other non-PPO related effects.

Figure 9b compares the two intermediate beat phases with the overall average. In both cases, the modulation

amplitude is largely comparable to the overall modulation amplitude. The slight differences in modulation amplitude may again be accounted for by the differing number of UVIS images going into each histogram, together with a possible bias due to varying image resolutions. However, the important detail in this figure is the phase shift of the two histograms compared to the overall average. As sketched in Figures 7c and 7d, we expect the auroral intensity peak to move to smaller Ψ_N if the southern PPO system is leading the northern (primary) one and to larger Ψ_N values for the opposite case—consistent with what we observe in Figure 9b.

5. Summary and Discussion

Following previous studies investigating PPO-modulation of Saturn's auroral emissions using HST UV imagery (Nichols et al., 2008, 2016; Nichols, Cowley, et al., 2010) and Cassini VIMS IR imagery (Badman, Andrews, et al., 2012), we employed the full Cassini UVIS data set to analyze the rotational modulation of Saturn's northern and southern UV aurora between 2007 and 2017. In order to avoid introducing a statistical bias due to the phase lock of the northern and southern PPO systems in near antiphase between mid-2013 and mid-2014, no data from this time window are included. This left us with 2,777 UVIS images which were used to qualitatively and quantitatively investigate modulations of the auroral intensity, due to the two PPO systems.

In both hemispheres, the auroral intensity was found to be strongly modulated by the primary PPO system (i.e., the system originating in the same hemisphere). The UV intensity generally maximizes close to $\Psi_N = 90°$ in the northern hemisphere and $\Psi_S = 270°$ in the southern hemisphere—coinciding with regions where upward FAC signatures have been observed (Andrews et al., 2010; Hunt et al., 2014). Concurrently, the intensities minimize on the opposite side of the pole where downward FACs have been observed. These intensity modulations are persistent throughout LT, albeit with varying modulation amplitudes in the dawn-noon and dusk-midnight regions.

Similarly, we observe clear UV auroral intensity modulations caused by the secondary PPO system (i.e., the system located in the opposite hemisphere) in both hemispheres. Again, intensity maxima (minima) are found close to where upward (downward) FAC currents associated with the secondary PPO systems have been observed to maximize (Bradley et al., 2018; Hunt et al., 2015)—with intensity maxima in the northern (southern) hemisphere occurring at about $\Psi_S = 90°$ ($\Psi_N = 270°$). Our observations are therefore clearly consistent with the present model of interhemispheric closure of PPO-associated currents (Bradley et al., 2018; Hunt et al., 2015). It seems as though the intensity modulation of the auroral emissions is slightly weaker for the secondary PPO systems than for the primary ones—indicating that not all PPO-associated currents close in the opposite hemisphere. Instead, this confirms that current closure must partly occur in the equatorial region just as observed by Bradley et al. (2018).

Interestingly, in both hemispheres and for both primary and secondary PPO modulations, the observed modulation of the UV auroral intensity is slightly phase shifted with respect to the sinusoidal modulation of FAC currents proposed by, for example, Hunt et al. (2014, 2015). This phase shift corresponds to an angular displacement of about 30–45° by which the observed auroral maxima and minima lag behind their expected locations. While we cannot readily explain this observation, we note that Hunt et al. (2014) found the upward FACs associated with the primary PPO system in the southern hemisphere to maximize at around $\Psi_S = 300°$—lagging the model expectation by about 30° as well. However, this analysis could be performed neither for the northern hemisphere or for interhemispheric modulations due to the complexity of the data set. Relying on this one analysis though, we can assume that the FAC and UV emission maxima are colocated and altogether lagging the model proposed by Andrews et al. (2010; see their Figure 12). Furthermore, it is worth pointing out that the FACs they observed in the equatorial plane are by no means as clearly organized as this first-order model assumes—the lag we observe in the UV auroral intensity is therefore well within the prediction error of this model.

A more in-depth analysis of the intensity modulation of the northern UV aurora during different relative orientations of the two PPO systems (beat phases) shows the expected higher (lower) modulation amplitude when the two systems are in phase (in antiphase); the expected phase shift of the modulation during times when the southern PPO system is leading/lagging the northern PPO system is also clearly observable. This serves as further proof that both the FACs associated with the primary and secondary PPO systems flow on the same field lines and that the auroral intensity depends on the combined current density of the two.

Overall, the UV auroral intensity observations analyzed in this study clearly support observations of FAC flows in both hemispheres. Despite some offsets between the locations of FAC maxima proposed by the initial simple model by Andrews et al. (2010) and the intensity maxima observed in auroral emissions, the results of this investigation provide the best overall evidence to date in auroral data for the application of the present simple PPO model (e.g., Andrews et al., 2010; Bradley et al., 2018; Hunt et al., 2014, 2015). This highlights the importance of continuous auroral observations for tracking PPO-related features on Saturn, as large data sets are required to successfully perform the necessary statistical analyses.

Acknowledgments
UVIS data are available from the NASA Planetary Data System (https://pds.jpl.nasa.gov). All PPO phase data (2004–2017) are available on the University of Leicester Research Archive (http://hdl.handle.net/2381/42436). A. B. was funded by a Lancaster University FST studentship. J. K. and S. V. B. were supported by STFC grant ST/M001059/1. S. V. B. was also supported by an STFC Ernest Rutherford Fellowship ST/M005534/1. Work at the University of Leicester was supported by STFC Consolidated Grant ST/N000692/1. W. R. P. acknowledges support from the NASA JPL Cassini Project and Central Arizona College.

References

Andrews, D. J., Cowley, S. W. H., Dougherty, M. K., Lamy, L., Provan, G., & Southwood, D. J. (2012). Planetary period oscillations in Saturn's magnetosphere: Evolution of magnetic oscillation properties from southern summer to post-equinox. *Journal of Geophysical Research*, *117*, A04224. https://doi.org/10.1029/2011JA017444

Andrews, D. J., Cowley, S. W. H., Dougherty, M. K., & Provan, G. (2010). Magnetic field oscillations near the planetary period in Saturn's equatorial magnetosphere: Variation of amplitude and phase with radial distance and local time. *Journal of Geophysical Research*, *115*, A04212. https://doi.org/10.1029/2009JA014729

Badman, S. V., Achilleos, N., Arridge, C. S., Baines, K. H., Brown, R. H., Bunce, E. J., et al. (2012). Cassini observations of ion and electron beams at Saturn and their relationship to infrared auroral arcs. *Journal of Geophysical Research*, *117*, A01211. https://doi.org/10.1029/2011JA017222

Badman, S. V., Andrews, D. J., Cowley, S. W. H., Lamy, L., Provan, G., Tao, C., et al. (2012). Rotational modulation and local time dependence of Saturn's infrared H_3^+ auroral intensity. *Journal of Geophysical Research*, *117*, A09228. https://doi.org/10.1029/2012JA017990

Badman, S., Masters, A., Hasegawa, H., Fujimoto, M., Radioti, A., Grodent, D., et al. (2013). Bursty magnetic reconnection at Saturn's magnetopause. *Geophysical Research Letters*, *40*, 1027–1031. https://doi.org/10.1002/grl.50199

Belenkaya, E. S., Cowley, S. W. H., Meredith, C. J., Nichols, J. D., Kalegaev, V. V., Alexeev, I. I., et al. (2014). Magnetospheric magnetic field modelling for the 2011 and 2012 HST Saturn aurora campaigns—Implications for auroral source regions. *Annales Geophysicae*, *32*(6), 689–704. https://doi.org/10.5194/angeo-32-689-2014

Belenkaya, E. S., Cowley, S. W. H., Nichols, J. D., Blokhina, M. S., & Kalegaev, V. V. (2011). Magnetospheric mapping of the dayside UV auroral oval at Saturn using simultaneous HST images, Cassini IMF data, and a global magnetic field model. *Annales Geophysicae*, *29*(7), 1233–1246. https://doi.org/10.5194/angeo-29-1233-2011

Bradley, T. J., Cowley, S. W. H., Provan, G., Hunt, G. J., Bunce, E. J., Wharton, S. J., et al. (2018). Field-aligned currents in Saturn's nightside magnetosphere: Subcorotation and planetary period oscillation components during northern spring. *Journal of Geophysical Research: Space Physics*, *123*, 3602–3636. https://doi.org/10.1029/2017JA024885

Brandt, P. C., Khurana, K. K., Mitchell, D. G., Sergis, N., Dialynas, K., Carbary, J. F., et al. (2010). Saturn's periodic magnetic field perturbations caused by a rotating partial ring current. *Geophysical Research Letters*, *37*, L22103. https://doi.org/10.1029/2010GL045285

Carbary, J. F. (2013). Longitude dependences of Saturn's ultraviolet aurora. *Geophysical Research Letters*, *40*, 1902–1906. https://doi.org/10.1002/grl.50430

Carbary, J. F., & Mitchell, D. G. (2013). Periodicities in Saturn's magnetosphere. *Reviews of Geophysics*, *51*, 1–30. https://doi.org/10.1002/rog.20006

Cowley, S. W. H., Bunce, E. J., & Prangé, R. (2004). Saturn's polar ionospheric flows and their relation to the main auroral oval. *Annales Geophysicae*, *22*(4), 1379–1394. https://doi.org/10.5194/angeo-22-1379-2004

Esposito, L. W., Barth, C. A., Colwell, J. E., Lawrence, G. M., McClintock, W. E., Stewart, A. I. F., et al. (2004). The Cassini ultraviolet imaging spectrograph investigation. *Space Science Reviews*, *115*(1–4), 299–361. https://doi.org/10.1007/s11214-004-1455-8

Galopeau, P., Zarka, P., & Le Queau, D. (1989). Theoretical model of Saturn's kilometric radiation spectrum. *Journal of Geophysical Research*, *94*(A7), 8739–8755. https://doi.org/10.1029/JA094iA07p08739

Gérard, J.-C., Bonfond, B., Gustin, J., Grodent, D., Clarke, J. T., Bisikalo, D., & Shematovich, V. (2009). Altitude of Saturn's aurora and its implications for the characteristic energy of precipitated electrons. *Geophysical Research Letters*, *36*, L02202. https://doi.org/10.1029/2008GL036554

Grodent, D., Gérard, J.-C., Cowley, S. W. H., Bunce, E. J., & Clarke, J. T. (2005). Variable morphology of Saturn's southern ultraviolet aurora. *Journal of Geophysical Research*, *110*, A07215. https://doi.org/10.1029/2004JA010983

Guo, R. L., Yao, Z. H., Wei, Y., Ray, L. C., Rae, I. J., Arridge, C. S., et al. (2018). Rotationally driven magnetic reconnection in Saturn's dayside. *Nature Astronomy*, *2*(8), 640–645. https://doi.org/10.1038/s41550-018-0461-9

Gurnett, D. A., Lecacheux, A., Kurth, W. S., Persoon, A. M., Groene, J. B., Lamy, L., et al. (2009). Discovery of a north-south asymmetry in Saturn's radio rotation period. *Geophysical Research Letters*, *36*, L16102. https://doi.org/10.1029/2009GL039621

Gustin, J., Grodent, D., Radioti, A., Pryor, W., Lamy, L., & Ajello, J. (2017). Statistical study of Saturn's auroral electron properties with Cassini/UVIS FUV spectral images. *Icarus*, *284*, 264–283. https://doi.org/10.1016/j.icarus.2016.11.017

Gustin, J., Grodent, D., Ray, L., Bonfond, B., Bunce, E., Nichols, J., & Ozak, N. (2016). Characteristics of north Jovian aurora from STIS FUV spectral images. *Icarus*, *268*, 215–241. https://doi.org/10.1016/j.icarus.2015.12.048

Hunt, G. J., Cowley, S. W. H., Provan, G., Bunce, E. J., Alexeev, I. I., Belenkaya, E. S., et al. (2014). Field-aligned currents in Saturn's southern nightside magnetosphere: Subcorotation and planetary period oscillation components. *Journal of Geophysical Research: Space Physics*, *119*, 9847–9899. https://doi.org/10.1002/2014JA020506

Hunt, G. J., Cowley, S. W. H., Provan, G., Bunce, E. J., Alexeev, I. I., Belenkaya, E. S., et al. (2015). Field-aligned currents in Saturn's northern nightside magnetosphere: Evidence for interhemispheric current flow associated with planetary period oscillations. *Journal of Geophysical Research: Space Physics*, *120*, 7552–7584. https://doi.org/10.1002/2015JA021454

Hunt, G. J., Cowley, S. W. H., Provan, G., Bunce, E. J., Alexeev, I. I., Belenkaya, E. S., et al. (2016). Field-aligned currents in Saturn's magnetosphere: Local time dependence of southern summer currents in the dawn sector between midnight and noon. *Journal of Geophysical Research: Space Physics*, *121*, 7785–7804. https://doi.org/10.1002/2016JA022712

Jackman, C. M., Achilleos, N., Cowley, S. W., Bunce, E. J., Radioti, A., Grodent, D., et al. (2013). Auroral counterpart of magnetic field dipolarizations in Saturn's tail. *Planetary and Space Science*, *82-83*, 34–42. https://doi.org/10.1016/j.pss.2013.03.010

Jackman, C. M., Provan, G., & Cowley, S. W. H. (2016). Reconnection events in Saturn's magnetotail: Dependence of plasmoid occurrence on planetary period oscillation phase. *Journal of Geophysical Research: Space Physics*, *121*, 2922–2934. https://doi.org/10.1002/2015JA021985

Jia, X., & Kivelson, M. G. (2012). Driving Saturn's magnetospheric periodicities from the upper atmosphere/ionosphere: Magnetotail response to dual sources. *Journal of Geophysical Research*, *117*, A11219. https://doi.org/10.1029/2012JA018183

Jia, X., Kivelson, M. G., & Gombosi, T. I. (2012). Driving Saturn's magnetospheric periodicities from the upper atmosphere/ionosphere. *Journal of Geophysical Research*, *117*, A04215. https://doi.org/10.1029/2011JA017367

Kinrade, J., Badman, S. V., Provan, G., Cowley, S. W. H., Lamy, L., & Bader, A. (2018). Saturn's northern auroras and their modulation by rotating current systems during late northern spring in early 2014. *Journal of Geophysical Research: Space Physics*, *123*, 6289–6306. https://doi.org/10.1029/2018JA025426

Kurth, W. S., Averkamp, T. F., Gurnett, D. A., Groene, J. B., & Lecacheux, A. (2008). An update to a Saturnian longitude system based on kilometric radio emissions. *Journal of Geophysical Research*, *113*, A05222. https://doi.org/10.1029/2007JA012861

Lamy, L., Prangé, R., Tao, C., Kim, T., Badman, S. V., Zarka, P., et al. (2018). Saturn's northern aurorae at solstice from HST observations coordinated with Cassini's grand finale. *Geophysical Research Letters*, *45*. https://doi.org/10.1029/2018GL078211

Meredith, C. J., Cowley, S. W. H., Hansen, K. C., Nichols, J. D., & Yeoman, T. K. (2013). Simultaneous conjugate observations of small-scale structures in Saturn's dayside ultraviolet auroras: Implications for physical origins. *Journal of Geophysical Research: Space Physics*, *118*, 2244–2266. https://doi.org/10.1002/jgra.50270

Mitchell, D., Carbary, J., Bunce, E., Radioti, A., Badman, S., Pryor, W., et al. (2016). Recurrent pulsations in Saturn's high latitude magnetosphere. *Icarus*, *263*, 94–100. https://doi.org/10.1016/j.icarus.2014.10.028

Nichols, J. D., Badman, S. V., Bunce, E. J., Clarke, J. T., Cowley, S. W. H., Hunt, G. J., & Provan, G. (2016). Saturn's northern auroras as observed using the Hubble Space Telescope. *Icarus*, *263*, 17–31. https://doi.org/10.1016/j.icarus.2015.09.008

Nichols, J. D., Cecconi, B., Clarke, J. T., Cowley, S. W. H., Gérard, J.-C., Grocott, A., et al. (2010). Variation of Saturn's UV aurora with SKR phase. *Geophysical Research Letters*, *37*, L15102. https://doi.org/10.1029/2010GL044057

Nichols, J. D., Clarke, J. T., Cowley, S. W. H., Duval, J., Farmer, A. J., Gérard, J.-C., et al. (2008). Oscillation of Saturn's southern auroral oval. *Journal of Geophysical Research*, *113*, A11205. https://doi.org/10.1029/2008JA013444

Nichols, J. D., Cowley, S. W. H., & Lamy, L. (2010). Dawn-dusk oscillation of Saturn's conjugate auroral ovals. *Geophysical Research Letters*, *37*, L24101. https://doi.org/10.1029/2010GL045818

Provan, G., Andrews, D. J., Cecconi, B., Cowley, S. W. H., Dougherty, M. K., Lamy, L., & Zarka, P. M. (2011). Magnetospheric period magnetic field oscillations at Saturn: Equatorial phase "jitter" produced by superposition of southern and northern period oscillations. *Journal of Geophysical Research*, *116*, A04225. https://doi.org/10.1029/2010JA016213

Provan, G., Cowley, S. W. H., Bradley, T. J., Bunce, E. J., Hunt, G. J., & Dougherty, M. K. (2018). Planetary period oscillations in Saturn's magnetosphere: Cassini magnetic field observations over the northern summer solstice interval. *Journal of Geophysical Research: Space Physics*, *123*, 3859–3899. https://doi.org/10.1029/2018JA025237

Provan, G., Cowley, S. W. H., Lamy, L., Bunce, E. J., Hunt, G. J., Zarka, P., & Dougherty, M. K. (2016). Planetary period oscillations in Saturn's magnetosphere: Coalescence and reversal of northern and southern periods in late northern spring. *Journal of Geophysical Research: Space Physics*, *121*, 9829–9862. https://doi.org/10.1002/2016JA023056

Provan, G., Cowley, S. W. H., Sandhu, J., Andrews, D. J., & Dougherty, M. K. (2013). Planetary period magnetic field oscillations in Saturn's magnetosphere: Postequinox abrupt nonmonotonic transitions to northern system dominance. *Journal of Geophysical Research: Space Physics*, *118*, 3243–3264. https://doi.org/10.1002/jgra.50186

Provan, G., Tao, C., Cowley, S. W. H., Dougherty, M. K., & Coates, A. J. (2015). Planetary period oscillations in Saturn's magnetosphere: Examining the relationship between abrupt changes in behavior and solar wind-induced magnetospheric compressions and expansions. *Journal of Geophysical Research: Space Physics*, *120*, 9524–9544. https://doi.org/10.1002/2015JA021642

Radioti, A., Grodent, D., Gérard, J.-C., Southwood, D. J., Chané, E., Bonfond, B., & Pryor, W. (2017). Stagnation of Saturn's auroral emission at noon. *Journal of Geophysical Research: Space Physics*, *122*, 6078–6087. https://doi.org/10.1002/2016JA023820

Southwood, D. J., & Chané, E. (2016). High-latitude circulation in giant planet magnetospheres. *Journal of Geophysical Research: Space Physics*, *121*, 5394–5403. https://doi.org/10.1002/2015JA022310

Yao, Z. H., Radioti, A., Rae, I. J., Liu, J., Grodent, D., Ray, L. C., et al. (2017). Mechanisms of Saturn's near-noon transient aurora: In situ evidence from Cassini measurements. *Geophysical Research Letters*, *44*, 11,217–11,228. https://doi.org/10.1002/2017GL075108

Zarka, P., Lamy, L., Cecconi, B., Prangé, R., & Rucker, H. O. (2007). Modulation of Saturn's radio clock by solar wind speed. *Nature*, *450*(7167), 265–267. https://doi.org/10.1038/nature06237